



CHALMERS
UNIVERSITY OF TECHNOLOGY

Uniaxial pressure induced stripe order rotation in $\text{La}_{1.88}\text{Sr}_{0.12}\text{CuO}_4$














Downloaded from: <https://research.chalmers.se>, 2024-06-29 21:15 UTC

Citation for the original published paper (version of record):

Wang, Q., von Arx, K., Mazzone, D. et al (2022). Uniaxial pressure induced stripe order rotation in $\text{La}_{1.88}\text{Sr}_{0.12}\text{CuO}_4$. Nature Communications, 13(1).
<http://dx.doi.org/10.1038/s41467-022-29465-4>

N.B. When citing this work, cite the original published paper.

Uniaxial pressure induced stripe order rotation in $\text{La}_{1.88}\text{Sr}_{0.12}\text{CuO}_4$

Qisi Wang ^{1✉}, K. von Arx ^{1,2}, D. G. Mazzone ³, S. Mustafi¹, M. Horio ¹, J. Küspert¹, J. Choi¹, D. Bucher¹, H. Wo⁴, J. Zhao ⁴, W. Zhang ⁵, T. C. Asmara ⁵, Y. Sassa², M. Månsson ⁶, N. B. Christensen⁷, M. Janoschek ^{1,8}, T. Kurosawa ⁹, N. Momono^{9,10}, M. Oda⁹, M. H. Fischer ¹, T. Schmitt ⁵ & J. Chang ^{1✉}

Static stripe order is detrimental to superconductivity. Yet, it has been proposed that transverse stripe fluctuations may enhance the inter-stripe Josephson coupling and thus promote superconductivity. Direct experimental studies of stripe dynamics, however, remain difficult. From a strong-coupling perspective, transverse stripe fluctuations are realized in the form of dynamic “kinks”—sideways shifting stripe sections. Here, we show how modest uniaxial pressure tuning reorganizes directional kink alignment. Our starting point is $\text{La}_{1.88}\text{Sr}_{0.12}\text{CuO}_4$ where transverse kink ordering results in a rotation of stripe order away from the crystal axis. Application of mild uniaxial pressure changes the ordering pattern and pins the stripe order to the crystal axis. This reordering occurs at a much weaker pressure than that to detwin the stripe domains and suggests a rather weak transverse stripe stiffness. Weak spatial stiffness and transverse quantum fluctuations are likely key prerequisites for stripes to coexist with superconductivity.

¹Physik-Institut, Universität Zürich, Winterthurerstrasse 190, CH-8057 Zürich, Switzerland. ²Department of Physics, Chalmers University of Technology, SE-412 96 Göteborg, Sweden. ³Laboratory for Neutron Scattering and Imaging, Paul Scherrer Institut, CH-5232 Villigen PSI, Switzerland. ⁴State Key Laboratory of Surface Physics and Department of Physics, Fudan University, Shanghai 200433, China. ⁵Photon Science Division, Swiss Light Source, Paul Scherrer Institut, CH-5232 Villigen PSI, Switzerland. ⁶Department of Applied Physics, KTH Royal Institute of Technology, SE-106 91 Stockholm, Sweden. ⁷Department of Physics, Technical University of Denmark, DK-2800 Kongens Lyngby, Denmark. ⁸Laboratory for Neutron and Muon Instrumentation, Paul Scherrer Institut, CH-5232 Villigen PSI, Switzerland. ⁹Department of Physics, Hokkaido University - Sapporo, 060-0810 Sapporo, Hokkaido, Japan. ¹⁰Department of Applied Sciences, Muroran Institute of Technology, Muroran 050-8585, Japan. ✉email: qisiwang@physik.uzh.ch; johan.chang@physik.uzh.ch

In the cuprates, stripes of doped holes—forming string-like antiferromagnetic domain walls that periodically modulate the charge density—have been both theoretically proposed^{1–8} and experimentally revealed⁹. The interplay between stripes and superconductivity is crucial¹⁰. Whereas static stripe order appears detrimental^{11,12}, fluctuating stripes may be favourable for superconductivity^{13–15}. Transverse stripe fluctuations, for example, have been theoretically suggested to promote superconductivity by enhancing the Josephson coupling between stripes¹³. While such meandering motions of stripes are driven by zero-point fluctuations¹³, they are also subject to a finite spatial stiffness, stemming from Coulomb repulsion and the underlying crystal lattice that defines the direction of the stripe order. In systems like the cuprates⁹, nickelates¹⁶ and manganites^{17,18}, charge-stripe order is thus usually pinned either parallel or diagonally to a principal atomic lattice axis.

In a strong-coupling picture, meandering stems from transverse excitations in the form of kinks shifting the stripes by an integer number of atomic units^{19,20}. On a macroscopic level, such kinks depin the stripe from the lattice. It has been suggested that the transverse stripe fluctuations have a crucial effect on the competition between charge order and superconductivity, and lead to a rich phase diagram featuring an electronic solid, an isotropic phase, and in between liquid crystal states coexisting with superconductivity¹³. However, direct experimental studies of charge-stripe dynamics remain challenging²¹. As yet, little is known about the lattice pinning potential and the transition from static to fluctuating meandering stripes.

Among hole-doped cuprate compounds, $\text{La}_{1.88}\text{Sr}_{0.12}\text{CuO}_4$ (LSCO) is unique because the orthorhombic lattice distortion is diagonal to the stripes, providing a less compatible lattice 'host'. In LSCO, the charge order is manifested by eight satellite reflections at $\mathbf{Q} = \boldsymbol{\tau} + \mathbf{q}_i$ ^{22,23}. Here, $\boldsymbol{\tau}$ is a fundamental Bragg peak and $\mathbf{q}_{1,2} = \pm(\delta_{\parallel}, \delta_{\perp})$ with $\delta_{\parallel} \approx 1/4$. The transverse incommensurability $\delta_{\perp} \approx 0.011$ is far beyond the expectation from orthorhombic twinning^{24–26}. The remaining six reflections appear at a mirror ($q_y \rightarrow -q_y$) and rotation ($q_x \rightarrow q_y$) symmetric equivalent positions. In the strong-coupling picture, the charge-stripe order is locally commensurate but with the possibility of phase jumping^{19,20,27,28}. The modulation δ_{\perp} is understood via kink ordering that effectively rotates the stripes away from the principle crystal axes. LSCO is thus a unique example of charge order “unlocked” from the lattice. As such, LSCO can be viewed as an intermediate stepping stone between statically pinned and fluctuating stripes.

Here, we study the transverse pinning properties of the charge-stripe order. For this purpose, we performed a resonant inelastic x-ray scattering (RIXS) experiment employing a uniaxial pressure application. Our setup enables weak in situ compressive strain along a copper-oxygen bond direction. We show how modest strain application gradually pins the stripe order to the crystal axis along the copper-oxygen bond direction, and thus demonstrate that uniaxial pressure allows tuning of kink ordering in LSCO. We find that the lattice pinning potential is weaker than that to detwin the stripe order. This suggests that, at least in LSCO, transverse stripe fluctuations possess an energy scale relevant for the ground state properties. The recent demonstration of uniaxial pressure tuning of electronic instabilities in combination with RIXS^{29,30} opens a new avenue for spectroscopy studies of quantum materials.

Results

Uniaxial pressure effect. Fig. 1 shows RIXS spectra recorded along the $(q_{\parallel}, 0)$ direction with and without strain application. The spectra reveal an elastic and low-energy ($\lesssim 1$ eV) paramagnetic

contribution and strong dd excitations at higher energy. The dd and the spin excitations show no discernible strain effect. This is in contrast to strain experiments on films. In La_2CuO_4 thin films, strain $\epsilon = (a - a_0)/a_0$ of the order $\sim 1\%$ yields a pronounced change of the dd excitations. A modification of the dd profile is easily detectable even with a strain of $\epsilon \sim 0.1\%$ (ref. 31). Similar results are reported on LaCoO_3 films³². Furthermore, the electronic and magnetic excitations in Sr_2IrO_4 thin films are sensitive to strain in the order of $\sim 0.2\%$ ³³. The absence of uniaxial pressure effects in our experiment suggests that the crystal field environment is only marginally modified³⁴. This is consistent with our strain calibration using x-ray diffraction (XRD) that yields an upper bound of the c -axis lattice expansion $\epsilon_c = (c - c_0)/c_0 \lesssim 0.015\%$ (see Methods, Supplementary Note 3 and Supplementary Fig. 2), which is at least an order of magnitude weaker than the maximum strain applied in ref. 35. Applying Poisson's ratio^{35,36}, we estimate the upper bound of the in-plane compressive strain $-\epsilon_b = (b - b_0)/b_0$ applied to be $\epsilon_b \lesssim 0.04\%$. Data in our work were obtained under three strain conditions with $\epsilon_{b,0} = 0$ and $0 < \epsilon_{b,1} < \epsilon_{b,2} < 0.04\%$.

This strain limit stems from the in situ operational screwdriver that provides finite mechanical force due to its magnetic coupling mechanism. Our strain cell (Fig. 1a) thus generates very modest uniaxial pressure. Away from $\mathbf{Q} = (\delta_{\parallel}, \pm\delta_{\perp})$, the strain has virtually no effect on the elastic and spin excitation scattering channels. The spectra obtained with and without uniaxial pressure are indistinguishable (Fig. 1d, f). At $\mathbf{Q} = (\delta_{\parallel}, 0)$ by contrast, elastic scattering is significantly increased after the application of pressure (Fig. 1e).

Stripe order (de)pinning. RIXS spectra are fitted by modelling elastic and magnon scattering with a Gaussian and a damped harmonic oscillator functional form, respectively³⁷ (Fig. 1d–f). The Gaussian width is fixed to the instrumental resolution. Fig. 2d–f displays RIXS intensity as a function of momentum and energy loss. Elastic intensity is obtained by integrating the spectral weight around zero energy within \pm FWHM energy window (black dashed lines, see Methods for details). The resulting longitudinal $(q_{\parallel}, 0)$ and transverse $(\delta_{\parallel}, q_{\perp})$ scans are plotted in Fig. 2g–l. Under ambient pressure conditions, elastic scattering peaks appear at $(\delta_{\parallel}, \pm\delta_{\perp})$ ^{24,38,39}, resulting in a double-peak structure in the transverse scan (Fig. 2d, g). Upon application of uniaxial pressure, δ_{\parallel} remains unchanged (Fig. 2j–l). By contrast, the transverse incommensurability δ_{\perp} is highly sensitive to uniaxial pressure and quickly vanishes upon pressure application (Fig. 2g–i). This results in a transverse scan that features a single peak structure centred around $(\delta_{\parallel}, 0)$. The same effect is found along the perpendicular copper-oxygen bond direction (Fig. 3a, b). Modest uniaxial pressure thus generates a twinned charge order structure with ordering vectors $(\delta_{\parallel}, 0)$ and $(0, \delta_{\parallel})$. As shown in Supplementary Fig. 4, the stripe order remains pinned after releasing uniaxial pressure. It is possible that uniaxial pressure triggers a meta-stable crystal structure which stabilises the pinning of stripe order. Within statistical errors, the correlation lengths (longitudinal ξ_{\parallel} and transverse ξ_{\perp}) display no change upon application of uniaxial pressure (Fig. 2m). Furthermore, we find isotropic correlation lengths $\xi_{\parallel} \approx \xi_{\perp}$.

Temperature dependence. After obtaining the pinned charge-stripe order, we studied its temperature evolution with uniaxial strain released. With increasing temperature, the charge order peak amplitude I decreases in a $T^{-\eta}$ fashion with $\eta \approx 8/5$ (Fig. 3c–f) up to the highest measured temperature of 120 K. The correlation length roughly scales with peak amplitude as $I \sim \xi^2$ (see insets of Fig. 3f, g) and saturates around 20 Å in the high-

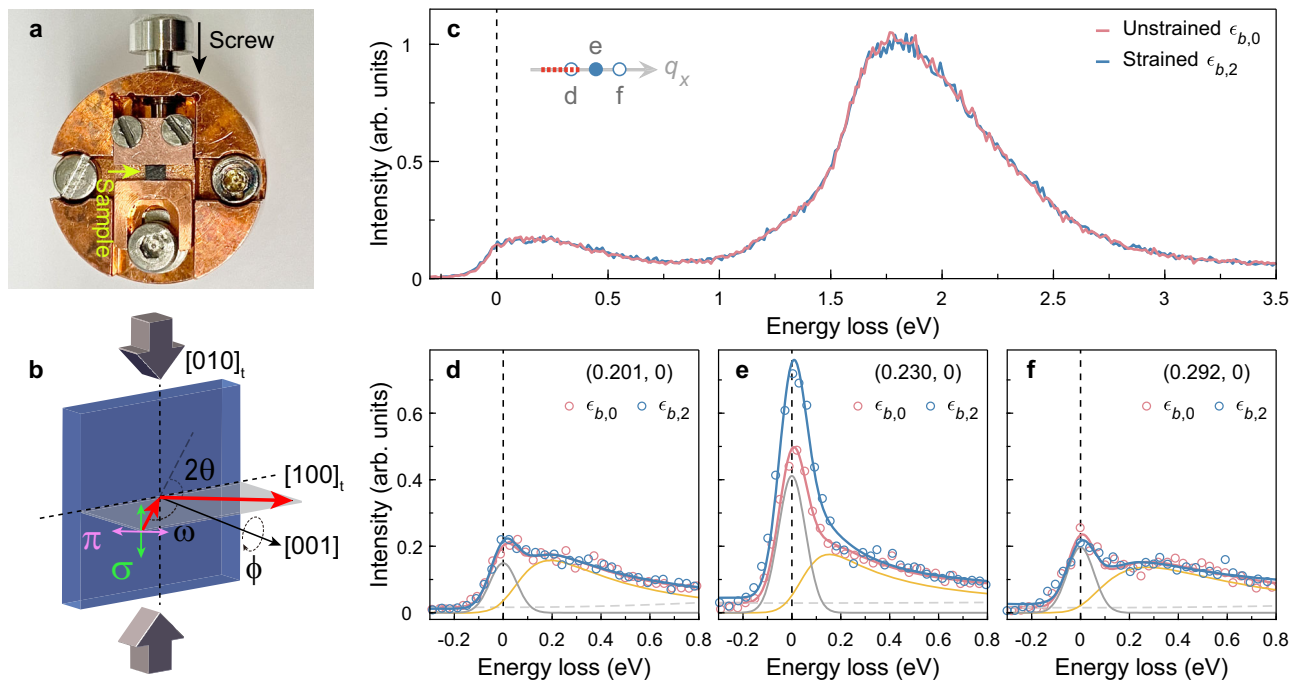


Fig. 1 Uniaxial strain tuning of charge-stripe order in $\text{La}_{1.88}\text{Sr}_{0.12}\text{CuO}_4$. **a** Photograph of the strain device—sample (black rectangle) and in situ mechanical screw mechanism are indicated with arrows. **b** Illustration of the scattering geometry with respect to the uniaxial strain application. Vertical (σ) and horizontal (π) linear light polarisations are indicated with respect to the scattering plane. **c** RIXS spectra including high-energy excitations recorded with (blue, $\epsilon_{b,2}$) and without (red, $\epsilon_{b,0}$) strain for $T \approx 28$ K. The inset indicates the momentum along $\mathbf{Q} = (q_{\parallel}, 0)$. The red dotted line reveals the momentum integration used for RIXS spectra in **c** and circles indicate the momenta for the RIXS spectra in **d-f**. **d-f** Low-energy part of RIXS spectra recorded with and without strain for momenta as indicated. Line profiles in **d-f** represent fits including a polynomial background (grey dashed line), a damped harmonic oscillator to model the paramagnetic contribution (orange line), and a Gaussian line shape covering the elastic scattering (grey solid line). The intensity is given in arbitrary units.

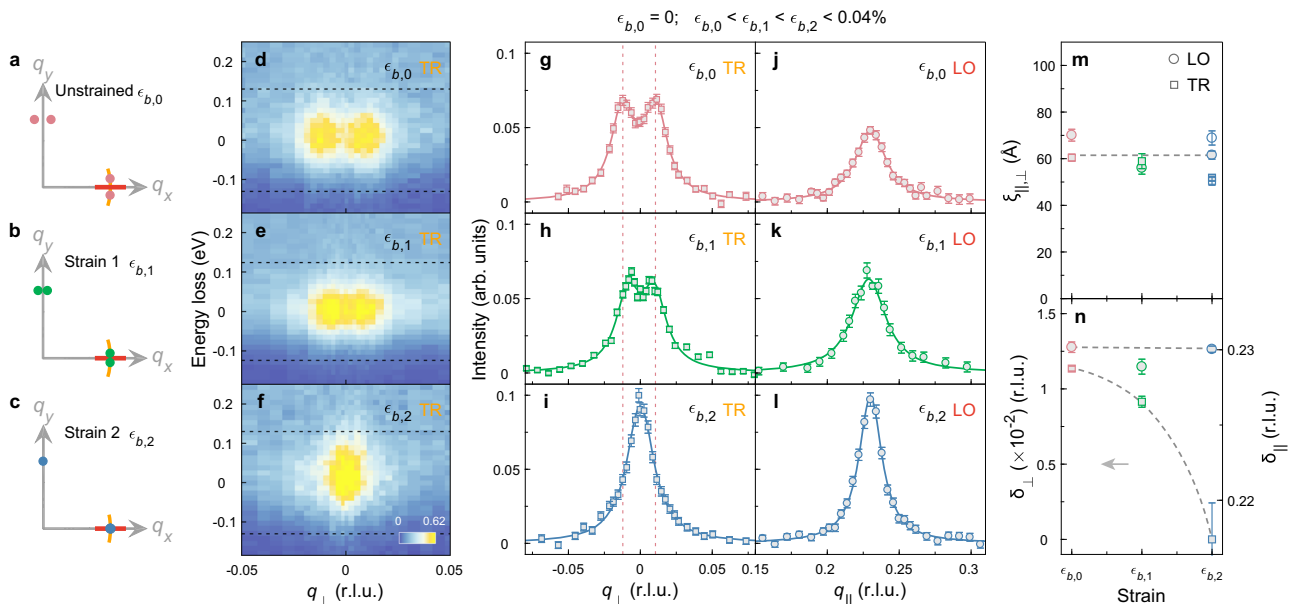


Fig. 2 Evolution of charge-stripe order structure in $\text{La}_{1.88}\text{Sr}_{0.12}\text{CuO}_4$ under uniaxial strain. **a-c** Illustration of the stripe order diffraction pattern as uniaxial pressure is increased. The splitting of stripe order peaks in **a, b** is exaggerated for clarity. Red and orange thick lines denote longitudinal (LO) and rocking (approximately transverse, TR) scans, respectively shown in **g-l** for $T = 28$ K $\approx T_c$. **d-f** RIXS intensity maps as a function of energy and q_{\perp} , from which scans in **g-i** are obtained. Black dashed lines, in **d-f**, mark the energy integration window of elastic intensity. Red dashed lines, in **g-i**, indicate the fitted peak positions of the transverse scan at zero strain. **m** Correlation length and **n** incommensurability along longitudinal and transverse directions extracted from fits (solid lines in **g-l**) as described in the main text and Supplementary Information. Open symbols in **m** denote results obtained on a repeated measurement with strain value comparable to strain 2. Error bars in **g-l** and **m, n** are set by counting statistics and standard deviation of fittings, respectively. Uniaxial pressure is increased from strain 1 ($\epsilon_{b,1}$) to strain 2 ($\epsilon_{b,2}$) by mechanically turning the screw pressing onto the sample. Strain 2 corresponds to the strain value for data shown in Fig. 1.

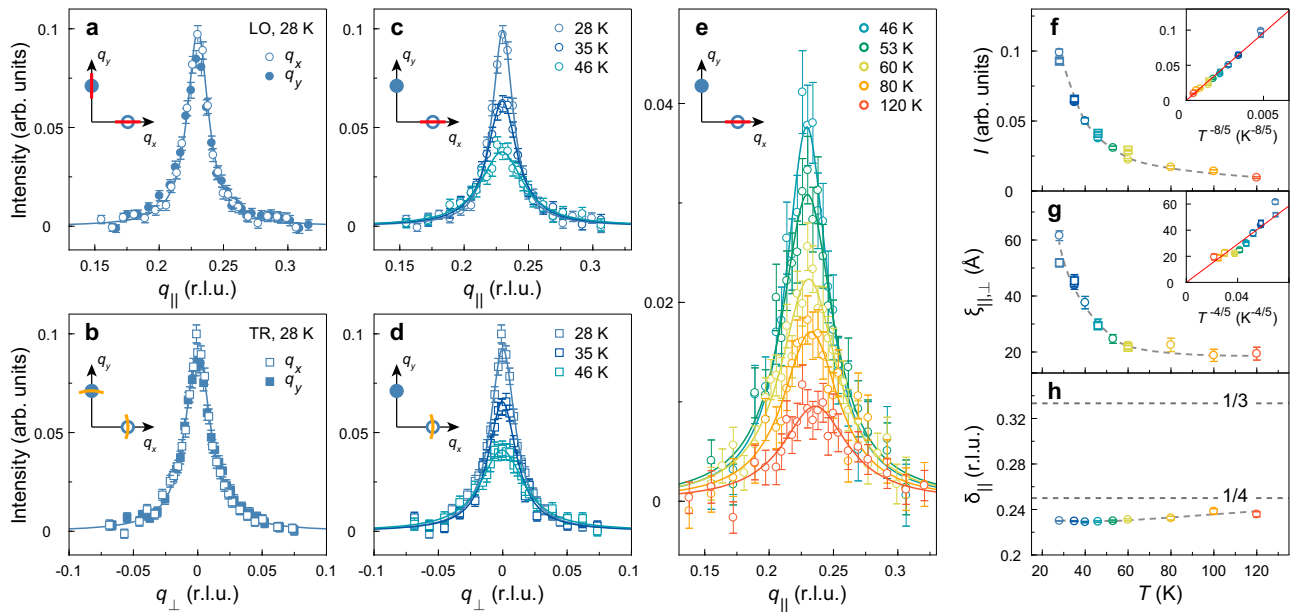


Fig. 3 Temperature evolution of lattice pinned charge-stripe order in $\text{La}_{1.88}\text{Sr}_{0.12}\text{CuO}_4$. **a** Longitudinal (circles) and **b** transverse (square) scans through the stripe ordering vectors at $T \approx T_c$. **c–e** Temperature dependence of the stripe order diffraction peaks. Solid lines in **a–e** are Lorentzian fits from which amplitude, correlation length and incommensurability are inferred and plotted in **f–h** versus temperature. Circles and squares in **f–h** denote fitting results from the longitudinal and transverse scans, respectively. Error bars in **a–e** and **f–h** are set by counting statistics and standard deviation of fittings, respectively. Dashed lines in **f, g** are guides to the eyes. The two horizontal dashed lines in **h** indicate lattice commensurate values. Red solid lines in the insets of **f, g** are linear fits.

temperature limit. Such a scaling behaviour was also revealed in $\text{La}_{0.165}\text{Eu}_{0.2}\text{Sr}_{0.125}\text{CuO}_4$ ³⁷ and therefore represents a universal characteristic of charge correlation in stripe-ordered cuprates. Finally, we find that the incommensurability δ_{\parallel} increases only marginally with temperature and never exceeds 1/4 within our probing window.

Discussion

To discuss the uniaxial pressure-induced stripe (de)pinning effect, we employ both a phenomenological Landau model^{40,41} and a strong-coupling real-space picture. Generally, a two-dimensional charge-density-wave modulation with wave vectors \mathbf{Q}_x and \mathbf{Q}_y is described by

$$\delta\rho(\mathbf{r}) = \text{Re}(\phi_x e^{i\mathbf{Q}_x \cdot \mathbf{r}}) + \text{Re}(\phi_y e^{i\mathbf{Q}_y \cdot \mathbf{r}}), \quad (1)$$

where $\delta\rho(\mathbf{r})$ is the spatial charge modulation and ϕ_i with $i = x, y$ are amplitudes. The Landau free energy density for these amplitudes in a tetragonal system is given by:

$$f_0 = \kappa_{\parallel}(|\partial_x \phi_x|^2 + |\partial_y \phi_y|^2) + \kappa_{\perp}(|\partial_y \phi_x|^2 + |\partial_x \phi_y|^2) + \alpha(|\phi_x|^2 + |\phi_y|^2) + \frac{\beta}{2}(|\phi_x|^2 + |\phi_y|^2)^2 - \gamma|\phi_x|^2|\phi_y|^2, \quad (2)$$

where the parameters α, β, γ describe the homogeneous phase, while κ_{\parallel} and κ_{\perp} link to the longitudinal and transverse stripe order stiffness. Spontaneous charge order emerges when $\alpha < 0$. Checkerboard and stripe orders are found for $\gamma > 0$ and $\gamma < 0$, respectively. The fourfold symmetry implies that both structures are manifested by reflections at $\mathbf{Q}_1 = (\delta_{\parallel}, 0)$ and $\mathbf{Q}_2 = (0, \delta_{\parallel})$. An orthorhombic distortion with B_{1g} or B_{2g} symmetry adds the following terms to the free energy density⁴⁰:

$$f_{\text{orth}} = -O_{ab}Q_a Q_b \bar{\phi}_a \phi_b + g(O_{ab}iQ_a \bar{\phi}_b \partial_b \phi_a + c.c.), \quad (3)$$

where $a, b = x, y$ and $O = h_{\parallel}\sigma_3$ or $O = h_{\perp}\sigma_1$ represents the B_{1g} or B_{2g} symmetry-breaking strain with $h_{\parallel(\perp)}$ and σ_j being the strain magnitude and the Pauli matrices, respectively. g is a phenomenological parameter and higher-order terms are neglected.

In absence of external strain, LSCO adopts the low-temperature orthorhombic structure with B_{2g} symmetry (see Fig. 4c). In this case, f_{orth} gives rise to a small rotation of the ordering vector away from the copper-oxygen bond direction with the new ordering vector being $\tilde{\mathbf{Q}} = |\mathbf{Q}|(1, gh_{\perp}/\kappa_{\perp})$. Such a transverse incommensuration is indeed observed^{24,25} (Fig. 2d, g). Application of external strain along the copper-oxygen bond direction promotes the B_{1g} symmetry-breaking terms with magnitude h_{\parallel} . For $h_{\parallel} \gg h_{\perp}$, detwinned stripe order pinned to the crystal lattice is expected and recently realised experimentally³⁵. With the modest uniaxial pressure applied in this study, we deem that $h_{\parallel} \leq h_{\perp}$. The observation of twinned stripe order with $\delta_{\perp} \rightarrow 0$ suggests that even modest uniaxial pressure induces a space group change of the crystal structure or reduced orthorhombic distortions. A recent numerical calculation using the Hubbard model shows that the stripe rotation is sensitive to the anisotropy of the next-nearest neighbour hopping⁴². This agrees with our finding that modest uniaxial pressure seems to induce an approximate tetragonal crystal field environment. The evolution from twinned depinned to detwinned pinned stripe order is depicted in Fig. 4c.

In the real-space view^{19,20,28}, the stripe incommensuration in unstrained LSCO corresponds to a slanted stripe phase with an average angle of $\sim 3^\circ$ rotated away from the crystal axis. A microscopic picture of the global incommensuration involves domain walls on stripes as elementary excitations of the order parameter¹⁹. Since any charge excitation along the stripe results in an increase in Coulomb energy, transverse excitations are therefore energetically favourable if the curvature energy—reflected by the transverse stiffness κ_{\perp} —is small. The model thus considers one-dimensional stripes as quantum strings with transverse kinks. It has been shown¹⁹ that inter-string coupling leads to a symmetry-breaking phase with directional kinks and thus slanted stripes. Internal or external B_{1g} orthorhombic strain could possibly increase the transverse stripe stiffness κ_{\perp} through

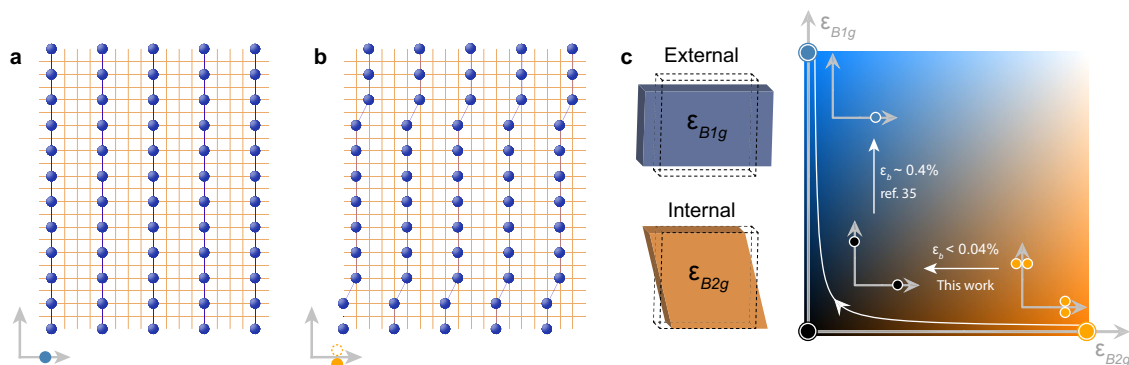


Fig. 4 Stripe order structures and strain phase diagram. **a, b** Schematic of half-filled, site-centred stripes. The orange grid represents the square CuO_2 lattice. Spheres illustrate the charge stripes. The in-between antiferromagnetic texture is not shown. **a** illustrates a statically pinned stripe order. Transverse kink ordering is illustrated in **b**. The density of aligned kinks along the stripes determines the transverse incommensurability δ_{\perp} . For unstrained LSCO, the density is about one kink every 20 copper sites. A schematic of the corresponding diffraction pattern is shown in the bottom-left corner. A dashed open circle indicates the position of charge order peak from the stripe twin domain rotating to the opposite direction. **c** Stripe order phase diagram as a function of orthorhombic B_{1g} and B_{2g} strain. The colour code indicates the parameter space coordinates $(gh_{\perp}/\kappa_{\perp}, gh_{\parallel}/\kappa_{\parallel})$, where gh_i with $i = \parallel, \perp$ represent orthorhombic strain and κ_i the stripe stiffness. Blue, black and orange phases represent pinned detwinned, pinned twinned and depinned twinned stripe order, respectively. White curve with arrow indicates schematically the connecting experiment trajectory upon application of uniaxial pressure. The straight white arrows indicate uniaxial pressure (this work and ref. ³⁵) applied to connect the different stripe order structures. Schematics on the left-hand side illustrate the two types of orthorhombic lattice distortions.

an enhanced electron-phonon coupling⁴³. The decrease of the transverse incommensurability $\delta_{\perp} \propto gh_{\perp}/\kappa_{\perp}$ is therefore likely a result of both the reduced B_{2g} orthorhombicity and enhanced stripe stiffness. On the other hand, the stripe density is reflected by the longitudinal modulation. The observation of longitudinal lattice incommensurability ($\delta_{\parallel} \neq 1/4$) may suggest the presence of stripe disorder (see Fig. 4a, b and Supplementary Fig. 6). The fact that δ_{\parallel} remains essentially unchanged upon application of modest uniaxial pressure indicates that the disorder potential is weakly dependent on pressure. Application of larger uniaxial pressure is known³⁵ to drive $\delta_{\parallel} \rightarrow 1/4$. In the quantum lattice string model, static stripes melt through a transverse kink proliferation^{20,28}, characterised by the transverse fluctuation magnitude¹³. Although the energy and time scales of the stripe dynamics^{14,21} are not directly resolved here, their prominent role is signified by the weak transverse stiffness revealed by our results. The fact that modest external strain stabilises the stripe phase suggests that LSCO is in the vicinity of a quantum melting point. The associated quantum fluctuations are likely crucial to the coexistence of superconductivity and stripe phase.

Methods

Samples. $\text{La}_{1.88}\text{Sr}_{0.12}\text{CuO}_4$ single crystals were grown by the floating zone method¹¹. The superconducting transition temperature is $T_c = 27$ K.

Resonant inelastic x-ray scattering. RIXS experiments were carried out at the ADDRESS beamline of the Swiss Light Source (SLS) at the Paul Scherrer Institut^{44,45}. The energy resolution—ranging from 124 to 130 meV—is estimated by the full-width-at-half-maximum (FWHM) of the elastic scattering peak from amorphous carbon tape. To enhance charge scattering, most data were taken using linear vertical (σ) incident light polarisation with grazing exit scattering geometry. Comparative measurements using horizontal (π) incident light polarisation have been performed under identical configurations (Supplementary Fig. 3). Wave vector $\mathbf{Q} = (q_x, q_y, q_z)$ is labelled in reciprocal lattice units (r.l.u.) of $(2\pi/a, 2\pi/b, 2\pi/c)$, where $a = b = 3.78$ Å and $c = 13.2$ Å are the lattice parameters of the high-temperature tetragonal unit cell. q_{\parallel} and q_{\perp} denote the longitudinal and transverse components of the in-plane momentum (q_x, q_y) in r.l.u., respectively. Samples were aligned with a and c axes in the horizontal scattering plane and b axis along the vertical direction. The scattering angle was fixed at $2\theta = 130^\circ$ (see Fig. 1b). In-plane momentum is set by varying the ω and ϕ angles (see Fig. 1b).

Uniaxial strain application. To apply uniaxial strain, we adapted a tool previously used to cleave crystals for angle-resolved photoemission spectroscopy

experiments⁴⁶. For the RIXS measurements, our LSCO crystals were cleaved using a top-post. Uniaxial pressure was applied at low temperature (~ 28 K) along a copper-oxygen bond direction through an in situ operational screw mechanism (see Fig. 1a).

Analysis of RIXS data. RIXS intensities are normalised to the weight of dd excitations³⁷. Elastic intensity is extracted by integrating the spectral weight around zero energy loss within \pm FWHM energy window. We have also analysed the data by defining the area of the fitted Gaussian elastic line as the elastic intensity. The two analysis methodologies yield consistent conclusions (Supplementary Figs. 7, 8). Correlation lengths are defined as the inverse half-width-at-half-maximum.

X-ray diffraction. XRD measurements were performed at 300 K where the uniaxial strain was applied. Since the elastic constants of the sample⁴⁷ and materials used for the strain cell (type 316 stainless steel⁴⁸ and copper⁴⁹) change only slightly below 300 K, the maximum strain values applied in the RIXS and XRD experiments are comparable.

Data availability

All data that support the findings of this study are available from the corresponding authors upon reasonable request. Source data are provided with this paper.

Received: 23 August 2021; Accepted: 16 March 2022;

Published online: 04 April 2022

References

- Machida, K. Magnetism in La_2CuO_4 based compounds. *Physica C* **158**, 192–196 (1989).
- Zaanen, J. & Gunnarsson, O. Charged magnetic domain lines and the magnetism of high- T_c oxides. *Phys. Rev. B* **40**, 7391–7394 (1989).
- Emery, V. & Kivelson, S. Frustrated electronic phase separation and high-temperature superconductors. *Physica C: Supercond.* **209**, 597–621 (1993).
- Castellani, C., Di Castro, C. & Grilli, M. Singular quasiparticle scattering in the proximity of charge instabilities. *Phys. Rev. Lett.* **75**, 4650–4653 (1995).
- Hellberg, C. S. & Manousakis, E. Phase separation at all interaction strengths in the t - J model. *Phys. Rev. Lett.* **78**, 4609–4612 (1997).
- Seibold, G., Sigmund, E. & Hizhnyakov, V. Unrestricted slave-boson mean-field approximation for the two-dimensional Hubbard model. *Phys. Rev. B* **57**, 6937–6942 (1998).
- Huang, E. W. et al. Numerical evidence of fluctuating stripes in the normal state of high- T_c cuprate superconductors. *Science* **358**, 1161–1164 (2017).
- Zheng, B.-X. et al. Stripe order in the underdoped region of the two-dimensional Hubbard model. *Science* **358**, 1155–1160 (2017).

9. Tranquada, J. M., Sternlieb, B. J., Axe, J. D., Nakamura, Y. & Uchida, S. Evidence for stripe correlations of spins and holes in copper oxide superconductors. *Nature* **375**, 561–563 (1995).
10. Emery, V. J. & Kivelson, S. A. Collective charge transport in high temperature superconductors. *Physica C: Supercond.* **235–240**, 189–192 (1994).
11. Chang, J. et al. Tuning competing orders in $\text{La}_{2-x}\text{Sr}_x\text{CuO}_4$ cuprate superconductors by the application of an external magnetic field. *Phys. Rev. B* **78**, 104525 (2008).
12. Hücker, M. et al. Stripe order in superconducting $\text{La}_{2-x}\text{Ba}_x\text{CuO}_4$ ($0.095 \leq x \leq 0.155$). *Phys. Rev. B* **83**, 104506 (2011).
13. Kivelson, S. A., Fradkin, E. & Emery, V. J. Electronic liquid-crystal phases of a doped Mott insulator. *Nature* **393**, 550–553 (1998).
14. Kivelson, S. A. et al. How to detect fluctuating stripes in the high-temperature superconductors. *Rev. Mod. Phys.* **75**, 1201–1241 (2003).
15. Scalapino, D. J. A common thread: the pairing interaction for unconventional superconductors. *Rev. Mod. Phys.* **84**, 1383–1417 (2012).
16. Tranquada, J. M., Buttrey, D. J., Sachan, V. & Lorenzo, J. E. Simultaneous ordering of holes and spins in $\text{La}_2\text{NiO}_{4.125}$. *Phys. Rev. Lett.* **73**, 1003–1006 (1994).
17. Shimomura, S., Wakabayashi, N., Kuwahara, H. & Tokura, Y. X-ray diffuse scattering due to polarons in a colossal magnetoresistive manganite. *Phys. Rev. Lett.* **83**, 4389–4392 (1999).
18. Vasilii-Doloc, L. et al. Charge melting and polaron collapse in $\text{La}_{1.2}\text{Sr}_{1.8}\text{Mn}_2\text{O}_7$. *Phys. Rev. Lett.* **83**, 4393–4396 (1999).
19. Bosch, M., van Saarloos, W. & Zaanen, J. Shifting bragg peaks of cuprate stripes as possible indications for fractionally charged kinks. *Phys. Rev. B* **63**, 092501 (2001).
20. Zaanen, J., Osman, O. Y. & van Saarloos, W. Metallic stripes: separation of spin, charge, and string fluctuation. *Phys. Rev. B* **58**, R11868(R) (1998).
21. Mitrano, M. et al. Ultrafast time-resolved x-ray scattering reveals diffusive charge order dynamics in $\text{La}_{2-x}\text{Ba}_x\text{CuO}_4$. *Sci. Adv.* **5**, eaax3346 (2019).
22. Croft, T. P., Lester, C., Senn, M. S., Bombardi, A. & Hayden, S. M. Charge density wave fluctuations in $\text{La}_{2-x}\text{Sr}_x\text{CuO}_4$ and their competition with superconductivity. *Phys. Rev. B* **89**, 224513 (2014).
23. Christensen, N. B. et al. Bulk charge stripe order competing with superconductivity in $\text{La}_{2-x}\text{Sr}_x\text{CuO}_4$ ($x = 0.12$). Preprint at <http://arxiv.org/abs/1404.3192> (2014).
24. Thampy, V. et al. Rotated stripe order and its competition with superconductivity in $\text{La}_{1.88}\text{Sr}_{0.12}\text{CuO}_4$. *Phys. Rev. B* **90**, 100510(R) (2014).
25. Kimura, H. et al. Incommensurate geometry of the elastic magnetic peaks in superconducting $\text{La}_{1.88}\text{Sr}_{0.12}\text{CuO}_4$. *Phys. Rev. B* **61**, 14366–14369 (2000).
26. Wakimoto, S. et al. Incommensurate lattice distortion in the high temperature tetragonal phase of $\text{La}_{2-x}(\text{Sr},\text{Ba})_x\text{CuO}_4$. *J. Phys. Soc. Jpn.* **75**, 074714 (2006).
27. McMillan, W. L. Theory of discommensurations and the commensurate-incommensurate charge-density-wave phase transition. *Phys. Rev. B* **14**, 1496–1502 (1976).
28. Eskes, H., Osman, O. Y., Grimberg, R., van Saarloos, W. & Zaanen, J. Charged domain walls as quantum strings on a lattice. *Phys. Rev. B* **58**, 6963–6981 (1998).
29. Kim, H.-H. et al. Charge density waves in $\text{YBa}_2\text{Cu}_3\text{O}_{6.67}$ probed by resonant x-ray scattering under uniaxial compression. *Phys. Rev. Lett.* **126**, 037002 (2021).
30. Lu, X. et al. Spin-excitation anisotropy in the nematic state of detwinned FeSe. Preprint at <http://arxiv.org/abs/2108.04484> (2021).
31. Ivashko, O. et al. Strain-engineering Mott-insulating La_2CuO_4 . *Nat. Commun.* **10**, 786 (2019).
32. Wang, R.-P. et al. Low-energy orbital excitations in strained LaCoO_3 films. *Phys. Rev. B* **100**, 165148 (2019).
33. Paris, E. et al. Strain engineering of the charge and spin-orbital interactions in Sr_2IrO_4 . *Proc. Natl Acad. Sci. USA* **117**, 24764–24770 (2020).
34. Moretti Sala, M. et al. Energy and symmetry of dd excitations in undoped layered cuprates measured by $\text{Cu } L_3$ resonant inelastic x-ray scattering. *New J. Phys.* **13**, 043026 (2011).
35. Choi, J. et al. Disentangling intertwined quantum states in a prototypical cuprate superconductor. Preprint at <https://arxiv.org/abs/2009.06967> (2020).
36. Meyer, T. L., Jiang, L., Park, S., Egami, T. & Lee, H. N. Strain-relaxation and critical thickness of epitaxial $\text{La}_{1.85}\text{Sr}_{0.15}\text{CuO}_4$ films. *APL Mater.* **3**, 126102 (2015).
37. Wang, Q. et al. High-temperature charge-stripe correlations in $\text{La}_{1.675}\text{Eu}_{0.2}\text{Sr}_{0.125}\text{CuO}_4$. *Phys. Rev. Lett.* **124**, 187002 (2020).
38. Ivashko, O. et al. Damped spin excitations in a doped cuprate superconductor with orbital hybridization. *Phys. Rev. B* **95**, 214508 (2017).
39. Wen, J. J. et al. Observation of two types of charge-density-wave orders in superconducting $\text{La}_{2-x}\text{Sr}_x\text{CuO}_4$. *Nat. Commun.* **10**, 3269 (2019).
40. Robertson, J. A., Kivelson, S. A., Fradkin, E., Fang, A. C. & Kapitulnik, A. Distinguishing patterns of charge order: stripes or checkerboards. *Phys. Rev. B* **74**, 134507 (2006).
41. Del Maestro, A., Rosenow, B. & Sachdev, S. From stripe to checkerboard ordering of charge-density waves on the square lattice in the presence of quenched disorder. *Phys. Rev. B* **74**, 024520 (2006).
42. He, W. et al. Prevalence of tilted stripes in $\text{La}_{1.88}\text{Sr}_{0.12}\text{CuO}_4$ and the importance of t' in the Hamiltonian. Preprint at <https://arxiv.org/abs/2107.10264> (2021).
43. Wang, Q. et al. Charge order lock-in by electron-phonon coupling in $\text{La}_{1.675}\text{Eu}_{0.2}\text{Sr}_{0.125}\text{CuO}_4$. *Sci. Adv.* **7**, eabg7394 (2021).
44. Ghiringhelli, G. et al. SAXES, a high resolution spectrometer for resonant x-ray emission in the 400–1600 eV energy range. *Rev. Sci. Instrum.* **77**, 113108 (2006).
45. Strocov, V. N. et al. High-resolution soft X-ray beamline ADDRESS at the Swiss Light Source for resonant inelastic X-ray scattering and angle-resolved photoelectron spectroscopies. *J. Synchrotron Radiat.* **17**, 631–643 (2010).
46. Månsson, M. et al. On-board sample cleaver. *Rev. Sci. Instrum.* **78**, 076103 (2007).
47. Migliori, A. et al. Elastic constants and specific-heat measurements on single crystals La_2CuO_4 . *Phys. Rev. B* **41**, 2098–2102 (1990).
48. Ledbetter, H. M. Stainless-steel elastic constants at low temperatures. *J. Appl. Phys.* **52**, 1587–1589 (1981).
49. Overton, W. C. & Gaffney, J. Temperature variation of the elastic constants of cubic elements. I. copper. *Phys. Rev.* **98**, 969–977 (1955).

Acknowledgements

We thank Ke-jin Zhou for the insightful discussions. Q.W., K.v.A., M.H., J.K., W.Z., T.C.A., T.S. and J.C. acknowledge support by the Swiss National Science Foundation through Grant Numbers BSSG10_155873, 200021_188564 and 200021_178867. K.v.A. is grateful for the support from the FAN Research Talent Development Fund-UZH Alumni. Q.W. and K.v.A. thank the Forschungskredit of the University of Zurich, under grant numbers [FK-20-128] and [FK-21-105]. T.C.A. acknowledges funding from the European Union's Horizon 2020 research and innovation programme under the Marie Skłodowska-Curie grant agreement No. 701647 (PSI-FELLOW-II-3i programme). Y.S. thanks the Chalmers Area of Advances-Materials Science and the Swedish Research Council (VR) with the starting grant (Dnr. 2017-05078) for funding. N.B.C. thanks the Danish Agency for Science, Technology, and Innovation for funding the instrument centre DanScatt and acknowledges support from the Q-MAT ESS Lighthouse initiative. M.M. is funded by the Swedish Research Council (VR) through a neutron project grant (Dnr. 2016-06955) as well as the KTH Materials Platform.

Author contributions

Q.W. and J. Chang conceived the project. T.K., N.M. and M.O. grew and characterised the LSCO single crystals. Q.W., J. Choi, D.B., M.M., and J. Chang designed the uniaxial strain device. Q.W., K.v.A., S.M., M.H., D.M., W.Z., T.C.A., Y.S., T.S. and J. Chang carried out the RIXS experiments. Q.W., H.W. and J.Z. performed the XRD measurements. Q.W. and J. Chang analysed the data with support from J.K., N.B.C., M.H.F. and M.J. Q.W. and J. Chang wrote the manuscript with input from all authors.

Competing interests

The authors declare no competing interests.

Additional information


Supplementary information The online version contains supplementary material available at <https://doi.org/10.1038/s41467-022-29465-4>.

Correspondence and requests for materials should be addressed to Qisi Wang or J. Chang.

Peer review information *Nature Communications* thanks the anonymous, reviewer(s) for their contribution to the peer review of this work.

Reprints and permission information is available at <http://www.nature.com/reprints>

Publisher's note Springer Nature remains neutral with regard to jurisdictional claims in published maps and institutional affiliations.

 **Open Access** This article is licensed under a Creative Commons Attribution 4.0 International License, which permits use, sharing, adaptation, distribution and reproduction in any medium or format, as long as you give appropriate credit to the original author(s) and the source, provide a link to the Creative Commons license, and indicate if changes were made. The images or other third party material in this article are included in the article's Creative Commons license, unless indicated otherwise in a credit line to the material. If material is not included in the article's Creative Commons license and your intended use is not permitted by statutory regulation or exceeds the permitted use, you will need to obtain permission directly from the copyright holder. To view a copy of this license, visit <http://creativecommons.org/licenses/by/4.0/>.

© The Author(s) 2022